Smart Structures and Systems, Vol. 5, No. 6 (2009) 633-644
DOI: http://dx.doi.org/10.12989/sss.2009.5.6.633

Detection of edge delamination in surface adhered active fiber composites

Dwo-Wen Wang and Ching-Chung Yin*

Department of Mechanical Engineering, National Chiao Tung University
1001 Ta Hsueh Road, Hsinchu 300, Taiwan, Republic of China

(Received January 2, 2009, Accepted May 13, 2009)

Abstract. A simple method has been developed to detect the bonding condition of active fiber composites (AFC) adhered to the surface of a host structure. Large deformation actuating capability is one of important features of AFC. Edge delamination in adhesive layer due to large interfacial shear stress at the free edge is typically resulted from axial strain mismatch between bonded materials. AFC patch possesses very good flexibility and toughness. When an AFC patch is partially delaminated from host structure, there remains sensing capability in the debonded part. The debonding size can be determined through axial resonance measured by the interdigitated electrodes symmetrically aligned on opposite surfaces of the patch. The electrical impedance and modal response of the AFC patch in part adhered to an aluminum plate were investigated in a broad frequency range. Debonding ratio of the AFC patch is in inverse proportion to the resonant frequency of the fundamental mode. Feasibility of in-*situ* detecting the progressive delamination between AFC patch and host plate is demonstrated.

Keywords: active fiber composite; delamination; electric impedance; resonance.

1. Introduction

Active fiber composites (AFC) are recently emerging functional materials used as integrated sensor/actuators in application of structural health monitoring (Schulz, *et al.* 2000, Datta, *et al*. 2003, Brunner, *et al.* 2005). Bent, *et al.* (1995) investigated the laminated structures actuated by anisotropic active materials such as monolithic PZT plate with in-plane poling yielded by surface interdigitated electrodes (IDE) and piezoelectric fiber composites polarized through the thickness. Both active materials were excited to induce planar deformation. Later, Bent and Hagood (1997) improved the performance of piezoelectric fiber composites to achieve large axial deformation by use of the d_{33} mode, in which IDE are placed on both surfaces of the patch to apply electric field for poling and subsequent actuation along the fibers. The current configuration of AFC is formed with unidirectional piezoelectric fibers embedded in epoxy matrix and sandwiched between two symmetrically aligned flexible printed circuit sheets with IDE. Fingers of those electrodes with alternating polarities are perpendicular to the piezoelectric fibers. Upon application of voltage to the surface electrodes, a periodically inverted electric field is induced in the interval between the adjacent electrode fingers. Axial extension or contraction can be performed in the patch and depends on the electric field applied in the direction along or opposite to the poling. The

*Associate Professor, Correspondence author, E-mail: ccyin@faculty.nctu.edu.tw

conformability of AFC allows for direct mounting on curved surfaces. AFC are sometimes called piezoelectric fiber composites (PFC). Macro Fiber Composites (MFC), developed by NASA (Wilkie, *et al.* 2000), are in the same family as AFC. The major difference between MFC and AFC is the cross section shape of piezoelectric fiber. The MFC uses rectangular cross section fibers whereas the AFC has round fibers. More contact area between the surface electrodes and the rectangular fibers reduces the attenuation of actuation electric field in MFC.

Material characteristics and possible applications of AFC have been studied intensively. Schulz, *et al.* (2000) utilized a long AFC tape with segmented electrodes as a distributed sensor integrated into a uniform cantilever beam. Detection of longitudinal stress wave was conducted to demonstrate the feasibility in application of structural health monitoring. Datta, *et al.* (2003) investigated the directional sensitivity of AFC for damage detection by capturing acoustic emission signals in composite beam. Brunner, *et al.* (2004) reported that AFC suited as replacement for conventional acoustic emission sensors. Brunner, *et al.* (2005) further concluded that AFC had very good potential in structural integrity assessment applications. The effect of applied strain level on integrated AFC in laminated composites was explored by Melnykowycz, *et al.* (2006). AFC sensor performance was discovered to be stable within the strain range below 0.20%. The AFC sensitivity degraded beyond a strain of 0.20% and approached a minimum at 0.50% strain. Cracking and subsequent fiber breakage is suspected to occur in the AFC if it is deformed over 0.20% strain.

Besides acting as acoustic transducers, AFC and MFC have been used to be active material components for vibration control (Wilkie, *et al*. 2000, Sodano, *et al.* 2004, Belloli, *et al.* 2004). Wickramasinghe and Hagood (2004) had AFC integrated into a composite blade spar laminate as active plies to perform structural control. These smart material functions are conducted as the AFC patch is firmly adhered to or integrated into a host structure. With improvement of manufacturing technology, large dimension AFC could be fabricated. Debonds between AFC patches and host structures are usually caused by unexpected voids at interfaces under discontinuous strains. The patch still possesses sensing and actuating capabilities if the patch is in part but not fully debonded from the host structure. The degradation must be determined for self tuning its performance. It results in a critical demand for effective in-*situ* inspection methods to assess the serviceability of AFC patches.

Seeley and Chattopadhyay (1998) experimentally investigated the effect of partially debonded PZT wafer on the structural response and in application of control. Their work focused on the changes of resonant frequencies and damping ratios when debonding size increased. Giurgiutiu, *et al*. (2002) exploited piezoelectric wafer as active sensors for structural health monitoring. The imaginary part of electrical impedance was used to distinguish the debonding conditions of sensors. Park, *et al.* (2006) demonstrated a self-diagnostic process to determine the functionality of piezoelectric sensor and bonding defects via electrical admittance measurement. Experimental results reveal that the upward shift in the slope of the imaginary part of the electrical admittance indicates the degree of debonding between PZT transducers and the host structure. On the other hand, sensor breakage results in a downward shift. The proposed diagnostic technique is based on the assumption that the mechanical impedance of the host structure is infinite. They concluded that a quantitative estimation of the bonding defect was required for obtaining a more detailed relation between bonding conditions and the degree of downward shift of admittance slope.

Axial actuation with large deformation is one of important features of AFC. Edge debonding in adhesive layer is typically caused by interfacial shear stress at the free edges due to mismatch of axial strains between bonded materials. Because of excellent flexibility and fracture toughness, the edge delaminated AFC patch could be supported by the remaining fully bonded portion. The patch is so thin that it has very small area moment of inertia. The delaminated patch is not able to resist large bending

moment without the backing of host structure. The symmetric layout of surface electrodes yields that only extensional strains in the debonded AFC can be excited by sinusoidal voltage and detected. The induced electric charge is proportional to the strain field experienced by piezoelectric fibers over coverage area of the electrodes. In this paper, the debonding length of AFC patch is determined by the measurement of electric impedance response associated with the extensional resonances. Further validations are conducted by analytic approach and FEM simulation on electric impedance response of the delaminated AFC patch elastically supported at one end.

2. Experiment and results

The AFC patches adopted in experiments were manufactured by Advanced Cerametrics, Inc. (Lambertville, New Jersey, USA). The piezoelectric fibers are made of PZT-5A powder by viscous suspension spinning process, abbreviated as VSSP (Cass, *et al*. 2003). The overall dimension is around 154 mm (length) × 15.3 mm (width) × 0.4 mm (thickness). Its active area is 128 mm (length) × 10 mm (width) with a number of 0.75 mm pitch IDE on opposite surfaces of each patch. The poling direction is parallel to the piezoelectric fibers and periodically inverted in the domain between adjacent electrodes. The electric field induced by electrode fingers with alternating polarities is applied in the direction along or opposite to its polarization. A simultaneous axial expansion or contraction is therefore performed in the entire unbonded AFC.

AFC is capable of bearing large axial deformation along the fiber direction. Interfacial shear stress and peel stress are induced in the adhesive layer because of the presence of discontinuous strains in the patch and the host structure. Similar phenomena due to thermal and stiffness mismatch of bonded materials are also found in adhesively bonded composite laminates (Delale, *et al.* 1981) or electronic assemblies (Wang, *et al.* 2000). The interfacial shear stress decays very fast from the free edge. The maximum interfacial shear stress probably yields edge debonds along the adhesive layer. Progressive interface cracking in edge area of the patch could result from weak bonding condition. The crack front is typically perpendicular to the fibers. One dimensional edge debonds are considered in this study. The debonded AFC patch is able to sense only in-plane extensional deformation because of its symmetric layout. No antisymmetric bending strain could be detected by the suspended AFC patch.

The AFC patches were adhered to a thick aluminum plate using Loctite E-120Hp epoxy-based adhesive with the vacuum bagging technique. The aluminum plate having a thickness of 5 mm is analogous to a stiff host structure. The edge delamination between the AFC patch and host structure was artificially made by placing a tape coated with silicone release agent underneath the prescribed portion. A schematic representation of the bonding configuration is shown in Fig. 1. The debonding length for consideration is in the range from 10 to 80% of active length of the patch. When the AFC patch is excited by a sinusoidal voltage with swept frequency, the maximum rate of electric charge leading to the local minimum electrical impedance occurs at every resonant frequency. The relative electrical impedances were measured by HP 8751A network analyzer (Agilent Technologies, Santa Clara, CA, USA) in the broad frequency range from 5 to 50 kHz and 50 to 100 kHz. A schematic view of experimental setup is illustrated in Fig. 2. The actual exciting voltage supplied by the network analyzer is less than 1 volt peak to peak. Only small-amplitude displacements would be induced in the AFC patch. The patch can not be damaged under such a low driving voltage. Each measurement had 801 data points within the frequency span and was converted to a text file for

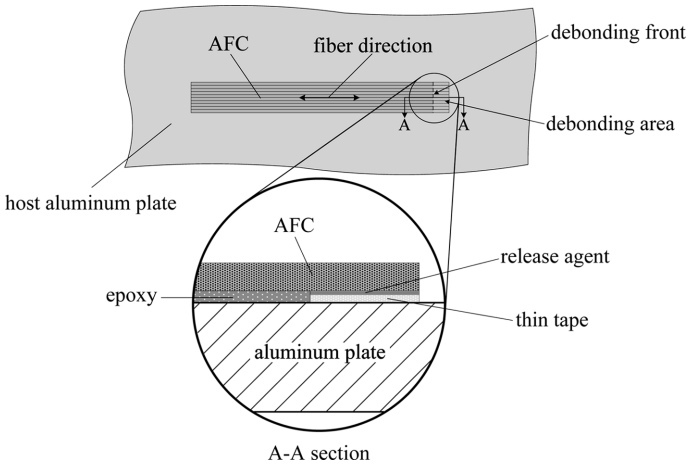

Fig. 1 Schematic view of bonding configuration for AFC patch

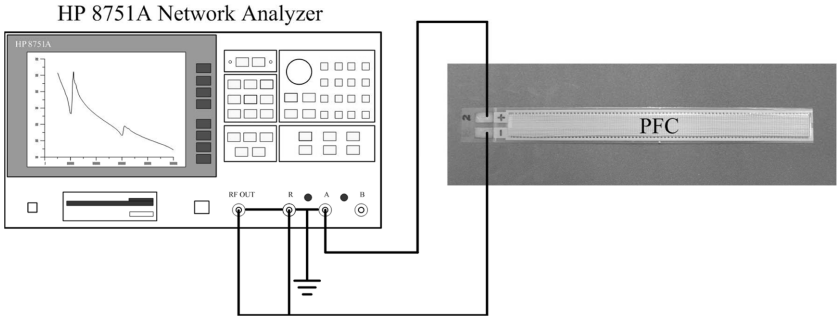

Fig. 2 Experimental setup used to perform impedance measurement for AFC

further analysis.

Fig. 3 depicts the measured electrical impedance curves. The impedance response recorded by HP 8751A is a relative rather than absolute value. Fig. 3(a) shows the impedance response of a free-free AFC patch measured before it was bonded to the aluminum plate. The first two resonant modes appear at 10.9 kHz and 31.4 kHz. After the AFC being adhered to the host plate the resonant modes disappear in the frequency range from 5 to 100 kHz. Fig. 3(b) shows the impedance response for fully bonded condition. The first resonant mode appears at 2,148 kHz, which is superior to the high frequency limit of observation. The response is monotonic decreasing in such frequency range.

Fig. 3(c) exhibits the impedance of a debonding AFC patch with 10% edge delamination. Its first mode occurs at 39.5 kHz. The impedance responses of those debonding AFC patches with 30%, 50%, and 70% debonding length are shown in Figs. 3(d), (e), and (f), respectively. Experimental evidence indicates that the resonant frequencies of the lowest three modes simultaneously decrease as the delamination ratio increase. The resonant frequency of fundamental mode is in inverse proportion to the debonding ratio of the AFC patch. In addition, the ratio of the second resonant frequency to the first one is a bit less then 3 (around 2.81 to 2.98) for debonding length ratio greater than 10%. Table 1 lists all the experimental results of electrical impedance measured on specimens.

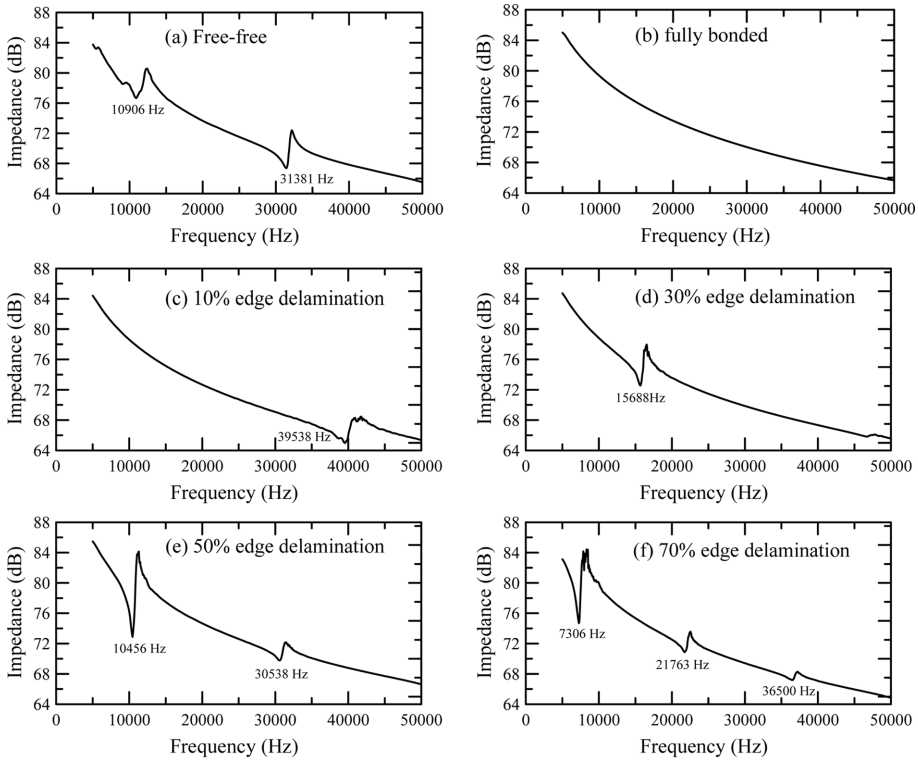

Fig. 3 Measured impedance curves for AFC patches with distinct debonding lengths

Table 1 Measured resonant frequencies for distinct debonding ratios to active length

ratio of debond condition	mode 1	mode 2	mode 3
10%	39,538 Hz		
20%	23,394 Hz	69,813 Hz	
30%	15,688 Hz	46,738 Hz	74,375 Hz
40%	13,269 Hz	37,288 Hz	62,000 Hz
50%	10,456 Hz	30,538 Hz	51,000 Hz
60%	8,656 Hz	25,531 Hz	42,406 Hz
70%	7,306 Hz	21,763 Hz	36,500 Hz
80%	6,406 Hz	18,500 Hz	31,044 Hz

3. Analytic approach

The AFC patch is constructed with a number of unidirectional piezoelectric fibers which are embedded in epoxy matrix and sandwiched between a pair of flexible sheets printed with IDE symmetrically aligned on the top and bottom surfaces. In the present study, the AFC patches were adhered to one side of an aluminum plate. As the AFC delaminated in part from the host plate is excited by a sinusoidal voltage, only extensional strains can be detected in the elastically suspended patch. Flexural and torsional vibrations in an unbonded AFC patch induce anti-symmetrically distributed axial strains. Neither bending nor torsional strains occurring in the debonded part of AFC could be measured by the surface

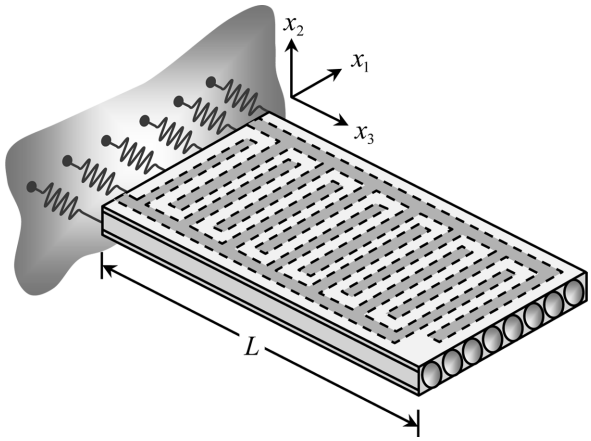

Fig. 4 Schematic diagram of analytical model for extensional vibration of AFC. Dashed lines indicate the IDE. The periodically inverted electric field induced by IDE is modeled as unidirectional electric field in the present one dimensional analysis

electrodes in symmetric layout.

Consider the debonded patch which has length L and is elastically supported at one end. Only axial stress in the x_3 direction is retained in the patch. Its schematic view was shown in Fig. 4. As mentioned previously, the AFC is assumed to have tangentially alternating poling in the domain between adjacent electrodes. Application of a periodically inverted electric field to the AFC leads to simultaneous axial expansion or contraction within the entire specimen. For simplicity, the AFC patch is modeled as a homogeneous piezoelectric material with unidirectional polarization and actuated by uniform electric field in theoretical formulation.

Using the IEEE compact matrix notation (ANSI/IEEE Std 176-1987), the constitutive equations related to normal stress components for piezoelectric materials with hexagonal symmetry are represented in the form.

$$T_1 = c_{11}^E S_1 + c_{12}^E S_2 + c_{13}^E S_3 - e_{31} E_3 \tag{1}$$

$$T_2 = c_{12}^E S_1 + c_{11}^E S_2 + c_{13}^E S_3 - e_{31} E_3 \tag{2}$$

$$T_3 = c_{13}^E S_1 + c_{13}^E S_2 + c_{33}^E S_3 - e_{33} E_3 \tag{3}$$

where T, S, E, c^{E}, e are the mechanical stress, the mechanical strain, the electric field, the elastic constant, the piezoelectric constant, respectively. The subscripts 1, 2 and 3 indicate the components of stress, strain, or electric field. The superscript E represents the quantity measured at the electric field which remains constant. Although the AFC is quite wide with respect to the thickness, the debonded patch is assumed to be slender. The lateral normal stress and shear stress components vanish in the entire debonded patch subjected to extensional vibration. There remains a non-zero axial stress described as $T_3 = \sigma_3$.

For free vibration of a slender AFC patch, its governing equation is

$$\frac{\partial \sigma_3}{\partial x_3} = \rho \frac{\partial^2 u_3}{\partial t^2} \tag{4}$$

in which ρ is the mass density of AFC. Combination of Eq. (1)-Eq. (4) results that

$$\bar{c}_{33}^{E}\frac{\partial^2 u_3}{\partial x_3^2}+\bar{e}_{33}\frac{\partial^2 \phi}{\partial x_3^2}=\rho\frac{\partial^2 u_3}{\partial t^2} \tag{5}$$

where ϕ denotes electric potential; $\bar{c}_{33}^{E}$ is the stiffened elastic constant and $\bar{e}_{33}$ is the effective piezoelectric constant. The latter two terms are defined by

$$\bar{c}_{33}^{E}=c_{33}^{E}-\frac{2(c_{13}^{E})^2}{c_{11}^{E}+c_{12}^{E}} \tag{6}$$

$$\bar{e}_{33}=e_{33}-\frac{2e_{31}c_{13}^{E}}{c_{11}^{E}+c_{12}^{E}} \tag{7}$$

The axial component of electric displacement for piezoelectric ceramics is

$$D_3=e_{31}(S_1+S_2)+e_{33}S_3+\varepsilon_{33}^{S}E_3 \tag{8}$$

The electric displacement D_3 has dimensions of electric charge per unit area. The AFC patch has relatively large aspect ratio of its axial length to its thickness. The electric field only applies in the axial direction. Therefore, shear strains S_4 and S_5 could be ignored during extensional vibration. Thus

$$\frac{\partial^2 \phi}{\partial x_3^2}=\frac{\bar{e}_{33}}{\bar{\varepsilon}_{33}^{S}}\frac{\partial^2 u_3}{\partial x_3^2} \tag{9}$$

where $\bar{\varepsilon}_{33}^{S}$ is effective dielectric constant expressed in the form

$$\bar{\varepsilon}_{33}^{S}=\varepsilon_{33}^{S}+\frac{2e_{31}^2}{c_{11}^{E}+c_{12}^{E}} \tag{10}$$

Substituting Eq. (9) into Eq. (5) leads to an equation of motion for extensional vibration of the debonded patch in the form

$$\left(\bar{c}_{33}^{E}+\frac{\bar{e}_{33}^2}{\bar{\varepsilon}_{33}^{S}}\right)\frac{\partial^2 u_3}{\partial x_3^2}=\rho\frac{\partial^2 u_3}{\partial t^2},\ 0<z<L \tag{11}$$

To simplify notation, $\bar{c}_{33}^{E}+(\bar{e}_{33}^2/\bar{\varepsilon}_{33}^{S})$ is denoted by $\overline{E}_3$. Consider the one dimensional extensional vibration model presented in Fig. 4. The AFC patch is suspended by linear elastic springs at one end and free of traction at the other end. The boundary conditions are described as follows:

$$ku_3(0)-A\bar{c}_{33}^{E}\left.\frac{\partial u_3}{\partial x_3}\right|_{x_3=0}=0,\ \left.\frac{\partial u_3}{\partial x_3}\right|_{x_3=L}=0 \tag{12}$$

where A denotes the cross-sectional area of the patch, k the effective linear spring constant of the elastic suspension. The frequency equation becomes

$$\tan(\beta L) = \frac{kL}{A\bar{c}_{33}^{E}}\frac{1}{\beta L} \tag{13}$$

with the parameter $\beta^2 = \rho\bar{E}_3^{-1}\omega^2$, ω indicates the angular frequency. The spring constant k of elastic suspension becomes infinitely large if the patch is clamped. Once the value of parameter $kL(A\bar{c}_{33}^{E})^{-1}$ approaches to infinity, the frequency equation degenerates to a vanishing cosine function in the form

$$\cos(\beta L) = 0 \tag{14}$$

The resonant frequencies f_r are expressed in ascending order as

$$f_r = \frac{r}{4}\sqrt{\frac{\bar{E}_3}{\rho L^2}}, \quad r = 1,3,5,... \tag{15}$$

One of the important characteristics of the extensional resonance is that higher harmonics are odd integer multiples of the fundamental resonant frequency.

In theoretical calculation of the extensional resonant frequencies, the delaminated patch was approximated by homogeneous piezoelectric ceramics PZT-5A, which has material properties close to AFC. Table 2 lists the properties of PZT-5A used in calculation. The analytical results for different ratios of edge debonding lengths are listed in Table 3. The lowest extensional harmonics are inversely proportional to the debonding ratio. The extensional resonant frequencies can be used to determine the debonding length of AFC patch delaminated from the host structure. It should be noted that the one dimensional analytic model is based on the hypotheses of unidirectional actuation electric field in the domain between IDE fingers as well as zero normal stress in the width direction. The assumptions are not longer valid in case the debonded patch has small length-to-width ratio. The normal strain in thickness

Table 2 Material properties of PZT-5A used in calculation

c_{11}^{E} (GPa)	120.4	ρ (kg/m^3)	7,600
c_{12}^{E} (GPa)	75.2	e_{31} (C/m^2)	-5.35
c_{13}^{E} (GPa)	75.1	e_{33} (C/m^2)	15.78
c_{33}^{E} (GPa)	110.9	e_{15} (C/m^2)	12.30
c_{44}^{E} (GPa)	21.1	$\varepsilon_{11}^{S}/\varepsilon_0$	919.05
c_{66}^{E} (GPa)	22.6	$\varepsilon_{33}^{S}/\varepsilon_0$	826.60

Table 3 Analytical resonant frequencies for different debonding ratios to active length

ratio of bebond	mode 1	mode 2	mode 3
10%	71,610 Hz	214,831 Hz	358,052 Hz
20%	35,805 Hz	107,415 Hz	179,026 Hz
30%	23,870 Hz	71,610 Hz	119,351 Hz
40%	17,903 Hz	53,708 Hz	89,513 Hz
50%	14,322 Hz	42,966 Hz	71,610 Hz
60%	11,935 Hz	35,805 Hz	59,675 Hz
70%	10,230 Hz	30,690 Hz	51,150 Hz
80%	8,951 Hz	26,854 Hz	44,756 Hz

induced by off axis electric field and the nonzero lateral stress have significant influence on axially extensional vibration. The ratios of higher harmonics to the fundamental one become a bit less than the corresponding odd integer multipliers. The deviation decreases if the debonding length of AFC patch is relatively large.

4. FEM simulation

A harmonic vibration analysis was carried out by using a commercial FEM code ANSYS 10.0 (ANSYS Inc., Canonsburg, PA, USA) to check validity of the hypothesis in analytic approach. The initial polarization and applied electric field underneath the electrodes are not parallel to the piezoelectric fibers. For simplicity, the influence of off-axis polarization on extensional vibration of AFC patch is ignored. The AFC patch was modeled as a periodically-inverted polarized PZT-5A strip sandwiched between symmetrically aligned electrodes. The piezoelectric brick element SOLID5 in ANSYS is adopted in computation. Each element has eight nodes and four degrees of freedom per node. The meshed model is composed of at most 1,300 elements in the fiber direction, 4 elements in the thickness, and at least 4 elements in the width. The delaminated AFC patch is fixed at one end and free at the other end. The IDE are considered again to include the influence of periodic electric field. But the mass of surface electrodes was neglected in FEM simulation. The voltage is directly applied to those nodes of meshes over the electrode coverage area.

Several cases with ratios of debonding lengths to the original active length varying from 10% to 80%

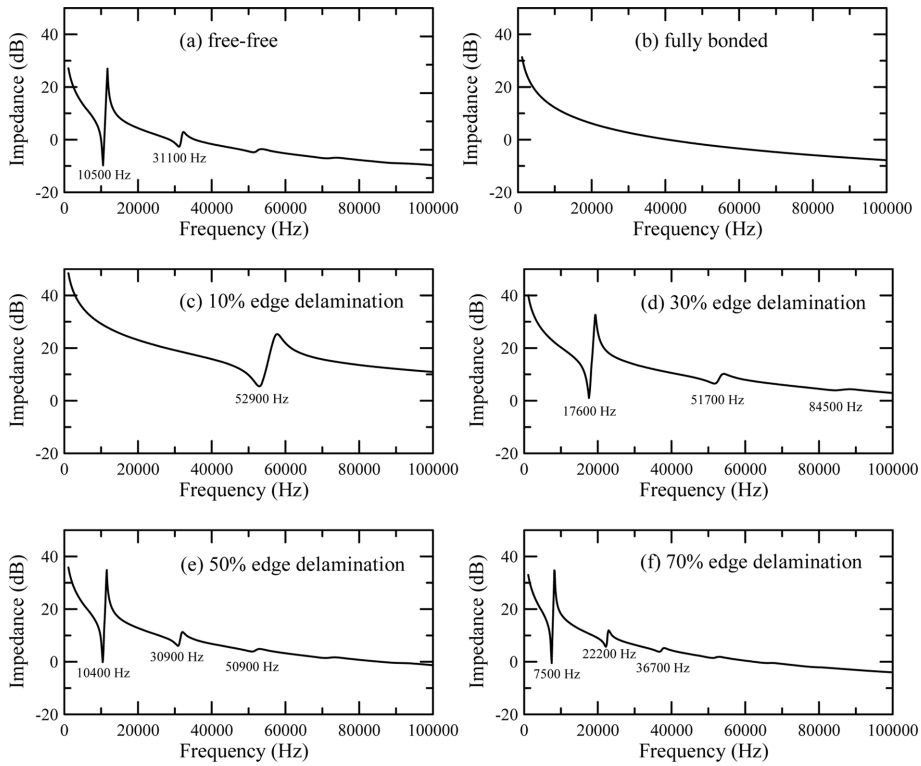

Fig. 5 Simulated impedance responses for delaminated patches by harmonic analysis

were considered. Fig. 5 shows the simulated impedance responses between two pads of the IDE on the AFC patches under free-free, fully bonded, and partially debonded conditions in a broad frequency range up to 100 kHz. The resonances occur at the local minima of electric impedance curves. Unfortunately, the magnitude of impedance predicted by FEM can not be directly compared with the relative value measured by network analyzer HP 8751A.

Fig. 5(a) depicts the calculated impedance response for an unbonded AFC patch with free boundary conditions at both ends. The lowest two resonant frequencies of extensional vibration are 10.5 kHz and 31.1 kHz. The deviations between those predictions and the corresponding experimental data shown in Fig. 3(a) are 3.67% and 0.64%, respectively. The FEM simulation is thus assured to be valid for vibration analysis of debonding AFC patch. The peak-to-peak value of time harmonic voltage induced strain is 7.9 microstrains per volt at the fundamental resonance of the debonded patch with 10% debonding ratio. It was concluded by Melnykowycz, *et al.* (2006) that no cracking or subsequent fiber fragmentation would appear in the AFC patch below 0.20% strain. The small driving voltage supplied by network analyzer can not damage the AFC patch or influence the measured impedance results.

As shown in Fig. 5(b), fully bonded AFC patch has no resonance in the frequency range up to 1 MHz. Figs. 5(c)-(f) show the impedance curves of the patches with 10%, 30%, 50%, and 70% debonding length. For the above cases, the fundamental resonant frequencies appear at 52.9 kHz, 17.6 kHz, 10.4 kHz, and 7.5 kHz, respectively. The number of elements in width of the patch has been increased up to 12. However, the calculated resonant frequencies are close to the simulated results using 4 elements in width. It indicates that the predictions already converge stably. The simulated resonant frequencies have the same trend as the experimental results. The ratios of the higher harmonics to the fundamental harmonic are very near a sequence of odd integers. The numerical results agree with the special characteristics of extensional vibration of an elastic sheet. The resonant frequency of the fundamental mode decreases if debonding ratio of the AFC patch increases. The simulated resonant frequencies for different debonding ratios are listed in Table 4.

The resonant frequency of the fundamental mode is inversely proportional to the debonding ratio of the AFC patch. Fig. 6 displays the analytical and FEM simulated results of the fundamental resonant frequency with respect to the debonding ratio in comparison with the measured data. Good agreement is achieved for debonding length greater than 40% of the original. The resonant frequency of the patch with shorter debond is probably up to hundreds of kilo-hertz. The present analytic method for extensional vibration is a one- rather than two-dimensional model. It provides a clear idea to correlate the resonance data with the extensional vibration of debonded patch. However, the width to thickness ratio of the selected AFC patch is relatively large. The hypothesis of zero normal stress in lateral direction of the

Table 4 FEM simulated resonant frequencies for distinct debonding ratios to active length

ratio of bebond	mode 1	mode 2	mode 3
10%	52,900 Hz		
20%	26,400 Hz	76,500 Hz,	
30%	17,600 Hz	51,700 Hz	84,500 Hz
40%	13,200 Hz	38,900 Hz	64,100 Hz
50%	10,400 Hz	30,900 Hz	50,900 Hz
60%	8,700 Hz	25,800 Hz	42,700 Hz
70%	7,500 Hz	22,200 Hz	36,700 Hz
80%	6,500 Hz	19,400 Hz	32,200 Hz

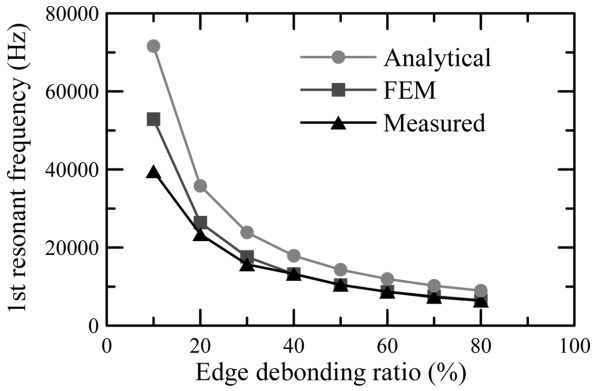

Fig. 6 Comparison between the measured and simulated results for the fundamental resonant frequencies versus debonding ratios of the patches

delaminated patch is suspected to yield the inevitable deviation between the analytical predictions and experimental data. The ratios of the lowest several resonant frequencies to the fundamental harmonic can be further used to distinguish the debonding length of AFC patch with shorter delamination from the host structure.

5. Conclusion

The AFC patch is capable of large deformation along the fibers and is used as a flexure actuator/sensor adhered to host structure. The discontinuous axial strains between bonded materials lead to interfacial shear stress induced edge debonds. The debonding length of edge delamination could be determined through the extensional resonance data. The extensional resonances of debonded AFC patch are measured from the electric impedance response upon application of a sinusoidal frequency sweep. The AFC is so thin that it has very small area moment of inertia. Without backing of a stiff host structure, the debonded AFC can not withstand large bending moment. The flexural resonances of AFC adhered to a host structure often appear in the bandwidth different from extensional resonances of the delaminated patch. In current study, the extensional harmonics of AFC patch occur in tens of kilohertz. There is no ambiguity in frequency responses between the extensional resonances of AFC and flexural vibrations of the entire structure. The very characteristics of extensional vibration on the debonded AFC patch are that the harmonics are in inverse proportion to the debonding length and in ascending sequence of odd integers.

Although a partially debonded patch still has both sensing and actuating capabilities, its performance is degraded due to edge delamination. To establish a complete network for monitoring the structural health, it is required to know the real-time situation of each sensor/actuator. The present method provides an effective way to assess the serviceability of each AFC patch according to the extensional resonant frequencies determined from electric impedance response. The electric fields are assumed to be unidirectional and alternating in analytic model as well as finite element approach. The electric field in the domain covered by surface electrodes is actually applied off axis to the fibers. However, the influence is neglected in modeling. There remains a critical issue of the accuracy limit due to the hypothesis. It is suspected that the differences between experimental and FEM results are caused by the

assumption of tangentially alternating electric field. The out-of-plane normal strain resulted from off axis poling and applied electric field underneath surface electrodes has influence on axial extension. Both analytic model and finite element approach give theoretical explanation for the nature behind the measured electric impedance associated with resonances of the AFC patch.

Acknowledgment

This research was supported in part by National Science Council of the Republic of China through grant NSC 96-2221-E-009-143. The authors thank the reviewers for their valuable comments.

References

ANSI/IEEE Std 176-1987, *IEEE Standard on Piezoelectricity*, IEEE, New York, NY.

Bent, A.A., Hagood, N.W. and Rodgers, J.P. (1995), "Anisotropic actuation with piezoelectric fiber composites", *J. Intel. Mat. Syst. Str.*, **6**, 338-349.

Bent, A.A. and Hagood, N.W. (1997), "Piezoelectric fiber composites with interdigitated electrodes", *J. Intel. Mat. Syst. Str.*, **8**, 903-919.

Brunner, A.J., Barbezat, M., Flüeler, P., Kornmann, X. and Huber, C. (2004), "Active fiber composites for application as acoustic emission sensors: principles and characterization", *DGZfP Proc. BB 90-CD*, Lecture, **54**, 549-556.

Brunner, A.J., Barbezat, M., Huber, C. and Flüeler, P.H. (2005), "The potential of active fiber composites made from piezoelectric fibers for actuating and sensing applications in structural health monitoring", *Mater. Struct.*, **38**, 561-567.

Cass, R.B., Khan, A. and Mohammadi, F. (2003), "Innovative ceramic-fiber technology energizes advanced cerametrics", *Am. Ceram. Soc. Bull.*, 9701-9706.

Datta, S., Kirikera, G.R., Schulz, M.J. and Sundaresan, M.J. (2003), "Continuous sensors for structural health monitoring", *Proc. of SPIE*, **5046**, 164-175.

Delale, F., Erodgan, F. and Aydinoglu, M.N. (1981), "Stresses in adhesively bonded joints: A close-form solution", *J. Compos. Mater.*, **15**, 249-271.

Giurgiutiu, V., Zagrai, A. and Bao, J.H. (2002), "Piezoelectric wafer embedded active sensors for aging aircraft structural health monitoring", *Struct. Health Monit.*, **1**(1), 41-61.

Melnykowycz, M., Kornmann, X., Huber, C., Barbezat, M. and Brunner, A.J. (2006), "Performance of integrated active fiber composites in fiber reinforced epoxy laminates", *Smart Mater. Struct.*, **15**, 204-212.

Park, G., Farrar, C.R., Rutherford, A.C. and Robertson, A.N. (2006), "Piezoelectric active sensor self-diagnostics using electrical admittance measurements", *J. Vib. Acoust.* ASME, **128**(4), 469-476.

Schulz, M.J., Sundaresan, M.J., Ghoshal, A. and Pai, P.F. (2000), "Active fiber composites for structural health monitoring", *Proc. of SPIE*, **3992**, 13-24.

Seeley, C.E. and Chattopadhyay, A. (1998), "Experimental investigation of composite beams with piezoelectric actuation and debonding", *Smart Mater. Struct.*, **7**, 502-511.

Sodano, H.A., Park, G. and Inman, D.J. (2004), "An investigation into the performance of macro-fiber composites for sensing and structural vibration applications", *Mech. Syst. Signal Pr.*, **18**, 683-697.

Wang, K.P., Huang, Y.Y., Chandra, A. and Hu, K.X. (2000), "Interfacial shear stress, peeling stress, and die cracking stress in trilayer electronic assemblies", *IEEE. T. Compon. Pack. T.*, **23**, 309-316.

Wickramasinghe, V.K. and Hagood, N.W. (2004), "Material characterization of active fiber composites for integral twist-actuated rotor blade application", *Smart Mater. Struct.,* **13**, 1155-1165.

Wilkie, W.K., Bryant, R.G., High, J.W., Fox, R.L., Hellbaum, R.F., Jalink, A., Little, Jr., B.D. and Mirick, P.H. (2000), "Low-cost piezocomposite actuator for structural control applications", *Proc. of 7th SPIE Int. Symposium on Smart Structures and Materials*, Newport Beach, CA, March 5-9.